HHS Public Access

Author manuscript

Wound Repair Regen. Author manuscript; available in PMC 2018 January 10.

Published in final edited form as:

Wound Repair Regen. 2017 September ; 25(5): 774–791. doi:10.1111/wrr.12584.

Mature B cells accelerate wound healing after acute and chronic diabetic skin lesions

Ruxandra F. Sîrbulescu, PhD[1,2], **Chloe K. Boehm**[1], **Erin Soon**[1], **Moses Q. Wilks, PhD**[2,3], **Iulian Ilieş, PhD**[4], **Hushan Yuan, PhD**[2,3], **Ben Maxner**[1], **Nicolas Chronos, MD**[1], **Charalambos Kaittanis, PhD**[2,3], **Marc D. Normandin, PhD**[2,3], **Georges El Fakhri, PhD**[2,3], **Dennis P. Orgill, MD, PhD**[5], **Ann E. Sluder, PhD**[1], and **Mark C. Poznansky, MB, ChB, PhD**[1,2]

[1]Vaccine and Immunotherapy Center, Division of Infectious Diseases, Department of Medicine, Massachusetts General Hospital, Boston, Massachusetts, USA

[2]Harvard Medical School, Boston, Massachusetts, USA

[3]Gordon Center for Medical Imaging, Nuclear Medicine and Molecular Imaging, Radiology Department, Massachusetts General Hospital, Boston, Massachusetts, USA

[4]Healthcare Systems Engineering Institute, College of Engineering, Northeastern University, Boston, Massachusetts, USA

[5]Division of Plastic Surgery, Brigham and Women's Hospital, Boston, Massachusetts, USA

Abstract

Chronic wounds affect 12–15% of patients with diabetes and are associated with a drastic decrease in their quality of life. Here we demonstrate that purified mature naïve $B220^+/CD19^+/IgM^+/IgD^+$ B cells improve healing of acute and diabetic murine wounds after a single topical application. B cell treatment significantly accelerated acute wound closure by 2–3 days in wild-type mice and 5–6 days in obese diabetic mice. The treatment led to full closure in 43% of chronic diabetic wounds, as compared to only 5% in saline-treated controls. Applying equivalent numbers of T cells or disrupted B cells failed to reproduce these effects, indicating that live B cells mediated pro-healing responses. Topically-applied B cell treatment was associated with significantly reduced scar size, increased collagen deposition and maturation, enhanced angiogenesis and increased nerve growth into and under the healing wound. β-III tubulin+ nerve endings in scars of wounds treated acutely with B cells showed increased relative expression of growth-associated protein 43. The improved healing associated with B cell treatment was supported by significantly increased fibroblast proliferation and decreased apoptosis in the wound bed and edges, altered kinetics of neutrophil infiltration, as well as an increase in TGF-β and a significant reduction in MMP2 expression in wound granulation tissue. Our findings indicate that the timeline and efficacy of wound healing can be experimentally manipulated through the direct application of mature, naive B cells, which effectively modify the balance of mature immune cell populations within the wound microenvironment and accelerate the healing process.

Correspondence should be addressed to R.F.S. (rsirbulescu@mgh.harvard.edu) or M.C.P. (mpoznansky@mgh.harvard.edu).

Conflicts of Interest: No competing financial interests exist.

INTRODUCTION

Effective and versatile technologies that facilitate acute and chronic wound healing remain a current unmet medical need. In the United States alone, chronic wounds affect an estimated 6.5 million patients, and numbers are expected to grow due to a sharp rise in the worldwide incidence of diabetes and obesity[1]. Cellular and tissue-based treatments that can simultaneously modulate inflammation in the wound microenvironment and promote regenerative responses have recently become a focus of wound care therapy development[2]. In healthy skin, wound healing is divided into four integrated and tightly regulated phases: hemostasis, inflammation, proliferation, and tissue remodeling[3]. Immune cells infiltrate the wound in a specific and predictable order, with neutrophils and macrophages associated with the inflammation phase, and lymphocytes associated with the proliferation and remodeling phases[4]. Chronic wounds are thought to become locked in the inflammatory stage of wound healing[5], with exaggerated proteolysis in the wound microenvironment mediating lesion stasis[6]. Moreover, the hypoxic conditions of the chronic wound bed degrade beneficial growth factors, preventing the progression towards the establishment of granulation tissue and extracellular matrix (ECM)[3] and full healing.

The role of lymphocytes in wound healing, particularly that of B cells, has received little attention[4]. However, recent studies indicate that B cells can act as powerful modulators of tissue regeneration[7]. In addition to their potential to differentiate into antibody-producing plasma cells, B cells can efficiently present antigens to T cells and modulate local immune responses through secretion of pro- and anti-inflammatory cytokines[8]. Interestingly, purified B lymphocytes applied exogenously to a lesion were demonstrated to support recovery. B cells isolated from bone marrow and directly inserted into sites of ischemic cardiac injury in a rat model increased cardiac function and tissue repair, performing better than CD117+ hematopoietic stem cells (HSCs)[9]. Studies that examined the impact of B cells in injury also describe beneficial effects on tissue healing. Splenectomized mice, in which the majority of mature B lymphocytes were removed, show delayed wound healing after skin lesions, while systemic reintroduction of isolated B cells rescued the wound healing phenotype[10]. An investigation using CD19-deficient animals suggested that hyaluronic acid within wounds may function as an endogenous ligand for toll-like receptor 4 (TLR-4) on the surface of B lymphocytes, triggering enhanced secretion of interleukin (IL)-6, IL-10 and transforming growth factor (TGF)-β, in a CD19-dependent manner[11]. These cytokines could in turn promote the production of growth factors within the tissue, aiding the healing process. In femoral fracture healing in mice, a system characterized by scarless regeneration, B cells massively infiltrated the callus region and actively promoted proliferative regeneration through secretion of osteoprotegerin[12].

We hypothesized that the introduction of relatively large numbers of B cells (approximately 80,000 cells/mm^3), which are typically present only in low numbers (approximately 100 cells/mm^3) and are associated with late, proliferative stages of wound healing, could accelerate and support tissue repair. Here, we show for the first time, to our knowledge, that isolated mature naïve B cells can accelerate skin wound closure and improve the quality of the regenerated tissue when applied topically onto the wound bed at the time of injury or after wound chronicization in validated mouse models of diabetic and non-diabetic acute and

chronic skin ulcers. B cell treatment was associated with reduced scarring and improved collagen deposition. Accelerated healing was supported by increased proliferation of wound fibroblasts in conjunction with decreased levels of apoptosis in the wound bed and edges and pro-regenerative modulation of cytokines and matrix metalloproteinases (MMPs). Acceleration of wound healing was not observed following the application of disrupted B cells, viable T cells, or hematopoietic stem cells.

MATERIALS AND METHODS

Mouse models

Wound healing studies were conducted in 7–9 weeks-old male wild-type C57Bl6/J mice and 8–65 weeks-old male B6.BKS(D) – *Lepr*^{db}/J mice (Jackson Laboratories). Male C57Bl6/J, B6.BKS(D) – *Lepr*^{db}/J, and FVB-Tg(CAG-luc,-GFP) L2G85Chco/J (all from Jackson Laboratories) were used as isogeneic donors for B and T cell isolation. Animals were maintained under standard laboratory care conditions, at temperatures ranging between 20–23°C, under a 12h:12h light:dark cycle, with ad libitum access to food and acidified water.

Lymphocyte isolation

Mouse spleens were collected in ice cold EasySep™ buffer (STEMCELL Technologies) containing 2% fetal bovine serum (FBS) and 1 mM ethylenediaminetetraacetic acid (EDTA) in phosphate-buffered saline (PBS). Spleens were dissociated mechanically through a 40 μm cell strainer and the splenocyte suspension was processed for negative B or T cell selection through immunomagnetic separation and retention of non-target cells, using commercially available cell isolation kits (STEMCELL Technologies, Inc.) according to the manufacturer's instructions. HSC isolation was performed through positive selection and immunomagnetic separation using CD117 MicroBeads, a MiniMACS™ separator, and an MS column (Miltenyi Biotec, Inc.).

Flow cytometry analysis

To assess cell viability after the isolation procedure, the cells were first washed and re-suspended in PBS, and stained using a Zombie UV™ fixable viability kit according to the manufacturer's instructions (BioLegend, Inc.). The stained cells were washed and re-suspended in PBS containing 1% FBS and 0.01% sodium azide (RICCA Chemical), blocked with FcR blocking reagent (Miltenyi Biotec) at 10 μl/10^6 cells, then incubated with the following primary antibodies for 30 minutes at 4°C: FITC-conjugated rat anti-mouse IgM (clone RMM-1), Brilliant Violet 605™-conjugated rat anti-mouse IgD (clone 11–26c.2a), Brilliant Violet 421™-conjugated rat anti-mouse CD19 (clone 6D5), APC-conjugated rat anti-mouse CD45R/B220 (clone RA3–6B2), PE-conjugated rat anti-mouse CD22 (clone OX-97), PE/Cy7-conjugated rat anti-mouse CD23 (clone B3B4), Brilliant Violet 510™-conjugated rat anti-mouse CD24 (clone M1/69), APC/Cy7-conjugated rat anti-mouse TER-119/erythroid cells (clone TER-119), Brilliant Violet 711™-conjugated rat anti-mouse CD3 (clone 17A2), Brilliant Violet 785™-conjugated hamster anti-mouse CD11c (clone N418), PE/Dazzle™ 594-conjugated rat anti-mouse CD117/c-Kit (clone 2B8) (all from BioLegend, Inc.), BUV395-conjugated hamster anti-mouse CD69 (clone H1.2F3), APC-R700-conjugated rat anti-mouse CD138 (clone 281-2) (all from BD Biosciences). The cells

were subsequently analyzed on an LSRFortessa X-20 flow cytometer (BD Biosciences) equipped with 355nm, 405nm, 488nm, 561nm, and 640nm laser lines. For each sample, at least 50,000 events were collected for analysis. Data were analyzed using FlowJo software, version 10.2 (TreeStar, Inc.).

Wound model and quantitation of healing

Full-thickness excisional wounds through the dorsal skin were induced as described previously[13]. Briefly, mice were anesthetized with a cocktail of ketamine (100 mg/kg) and xylazine (10 mg/kg), and the dorsal skin was shaved and depilated. Analgesia was provided pre-operatively with 0.08 mg/kg buprenorphine injected subcutaneously. The dorsal skin was tented and a 5-mm biopsy punch was passed through the skin fold, creating two symmetrical wounds on each side of the back. Each wound had an initial area of approximately 20 mm^2. Silicone splints with a square 14 mm by 14 mm outer profile and with an inner diameter of 7 mm were attached around the wounds using Vetbond tissue adhesive (3M). Cell suspensions in PBS or equal volumes of PBS solution alone (saline control) were applied directly onto the wound bed using a manual pipette. Each treated wound received 1.5×10^6 B cells or T cells (control) in 25 μl PBS. HSC controls received 12,000 purified HSCs per wound to replicate the maximum detected levels of CD117+ HSC contamination observed in negatively-selected B cell isolates (0.8%). The splinted wounds were then covered with Tegaderm™ transparent dressing (3M). High resolution photographs of the wounds (0.018 mm/pixel) were collected at regular intervals and the area of the open wound over time, as well as the area of the visible scar at the end point of each study were assessed using ImageJ software (National Institutes of Health). The splint area in each image was used to calibrate the measurements of the wound and to control for parallax error. Analysis of the wound areas was performed by experimenters blinded to the treatment conditions.

Histology

Wound biopsies at the end point of the wound healing time course were collected using a 10-mm biopsy punch and fixed in 4% paraformaldehyde in PBS for 24–48 hours at 4°C, after which the samples were dehydrated through graded ethanol and xylene washes, and embedded in paraffin. Transverse sections through the wound bed were cut at a thickness of 5 μm, and mounted onto microscopy slides. Serial sections were stained with hematoxylin and eosin and with Masson's trichrome stain for visualizing collagen fibers. Stained slides were digitized at a resolution of 0.25 μm/pixel using an Aperio CS2 scanner (Leica Biosystems). Digitized slides were used for scoring of tissue regeneration and neutrophil infiltration by observers blinded to the treatment conditions. For cellular infiltrate evaluation a minimum area of 3,500 μm^2 was examined in each wound region (wound bed, wound edge, and distal).

Immunohistochemistry and confocal imaging

Wound biopsies collected at 0 days (intact), 1 day, 4 days, and 16 days post-injury were fixed in 4% buffered paraformaldehyde for 24–48 hours at 4°C, then cryoprotected in 1M sucrose solution for another 24–48 hours at 4°C, and embedded in tissue freezing medium (Electron Microscopy Sciences). Transverse sections through the wound bed were cut at a thickness of 10 μm using a cryostat (Leica Biosystems), and thaw-mounted onto SuperFrost

Plus Gold slides (Fisher Scientific). For immunohistochemical detection of antigens, sections were washed through three changes of Tris-buffered saline (TBS) pH 7.4, then permeabilized and blocked by incubation for 1 hour at room temperature with TBS containing 5% bovine serum albumin, 5% FBS, and 0.3% Triton X-100. Sections were then incubated overnight at 4°C with the following primary antibodies diluted in blocking solution: allophycocyanin-conjugated rat anti-mouse CD45R/B220 (clone RA3–6B2; BioLegend, Inc.), phycoerythrin-conjugated rat anti-mouse CD31 (clone MEC 13.3; BD Biosciences), Alexa Fluor® 488-conjugated mouse anti-tubulin β3 (clone TUJ1; BioLegend, Inc.), Alexa Fluor® 594-conjugated mouse anti-MMP2 (clone M6303D01; BioLegend, Inc.), Alexa Fluor® 647 rat anti-mouse IL-10 (clone JES5–16E3; BioLegend, Inc.], rabbit polyclonal anti-mouse FGF2 (LifeSpan BioSciences), rat anti-mouse fibroblasts (clone ER-TR7; LifeSpan BioSciences), rabbit polyclonal anti-GAP43 (EMD Millipore), rat monoclonal anti-substance P (EMD Millipore), rabbit polyclonal anti-MMP8 (Bioss Antibodies), chicken polyclonal anti-TGF-β1 (Abcam), rabbit polyclonal anti-Ki67 (Abcam), and rabbit monoclonal anti-activated caspase 3 (clone C92–605; BD Pharmigen). Unbound primary antibody was removed by 3 rinses for 5 min each in TBS. If unconjugated primary antibodies were used, antigenic sites were visualized by incubating the sections for 2 hours at room temperature with Alexa Fluor 488®-conjugated F(ab')2- goat anti-rabbit IgG, Alexa Fluor 546®-conjugated goat anti-chicken IgY, or Alexa Fluor 555®-conjugated goat anti-rat IgG (all from Thermo Fisher Scientific), diluted 1:200 in blocking solution. Sections were counterstained by incubation with 2 μg/ml of 4′, 6-diamidino-2-phenylindoledihydrochloride (DAPI; Sigma Aldrich) in PBS for 3 min at room temperature. The sections were washed 3 times for 7 min in TBS and embedded using Fluoromount (Novus Biologicals). Antibody controls included incubation of the tissue sections with isotype antibodies and omission of the primary antibody when a secondary antibody was used for visualization. No unspecific signal was detected in the control samples.

Stained tissue sections were imaged using a Zeiss LSM 710 laser scanning microscope (Carl Zeiss) equipped with 20×, 40× and 63× objectives. Confocal images were taken at a resolution of 0.1–0.7 μm/pixel and an optical thickness of 0.5–2.2 μm using Zen software (Carl Zeiss).

Image analysis

Photographs of wounds as well as confocal microscopy images were analyzed using standard functions in ImageJ software (National Institutes of Health). In each photograph, the area of the open wound or the surface of the scar, respectively, as well as the area defined by the inner diameter of the silicone splint were measured manually. The known area of the splint was used to convert measurements from pixels to mm^2. Confocal images were used to assess cell proliferation, apoptosis, angiogenesis, and neuroregeneration. Cells and cell nuclei were quantified in ImageJ either manually, using the 'cell counter' function, or semi-automatically, by subtracting background and converting the image to binary, followed by watershed-based image segmentation to isolate discrete particles, which were then quantified using the 'analyze particles' function. Cell counts for specific markers were normalized to total cell counts based on DAPI counterstaining. For quantifying continuous structures, tissue fields of view were outlined manually within each image, and threshold values for

hue, saturation, and brightness were applied in order to select optimal intensity windows that unambiguously identified target structures. For quantifying intracellular expression, regions of interest were defined through intensity thresholding of DAPI counterstaining. The total area and mean labeling intensity of the target structures (blood vessels, nerve endings, or cells) was quantified using the 'analyze particles' or 'measure' functions, and normalized to the area of the analyzed region of interest. Images used for immunolabeling quantification were collected using identical confocal settings. All analyses were performed by observers blinded to the experimental conditions.

Micro-PET/CT imaging

Isolated splenic B cells were incubated for 3 hours at 37°C with protamine-conjugated ^{89}Zr Feraheme nanoparticles[14] at a concentration of 100 μg/ml iron. This incubation time was previously determined to be sufficient for labeling the majority of the B cells in suspension (data not shown). To remove unbound nanoparticle, the cells were centrifuged for 5 minutes at 500×g and re-suspended in fresh PBS three times, after which the cells were finally re-suspended in PBS at a concentration of 100,000 cells/μl. Approximately 2 million B cells in 20 μl of PBS, comprising 20 μCi of total radioactivity were applied the wound on the right dorsal side of the animal as described above, while the contralateral wound received an equal volume of PBS. The mice were imaged at regular intervals using an eXplore Vista micro-PET-CT imaging system (GE Healthcare). At the end point of the studies, the animals were euthanized and tissue samples from the treated wound site, the control wound, lymph nodes on each side of the body, the spleen, liver and muscle were collected for measuring residual radioactivity using a 2480 WIZARD^2 gamma counter (Perkin Elmer).

IVIS imaging

Splenic B cells were isolated from mice homozygous for the CAG-luc-eGFP L2G85 transgene, which show widespread expression of firefly luciferase and enhanced green fluorescence protein under the CAG promoter (Jackson Laboratories). Approximately 2.2 million luciferase-expressing B cells in PBS were applied to the wound on one side, as described above, while the contralateral wound received an equal volume of PBS. The mice were imaged using an IVIS Lumina II system (Caliper Life Sciences) on the day of the surgery and at regular intervals thereafter for a total of 4 weeks. For each imaging session, anesthesia was induced using 3% isoflurane in oxygen and maintained using 1 L/min of 2–3% isoflurane throughout the imaging session. To visualize luciferase activity, 50 μl of 30 mg/ml aqueous D-luciferin solution (Regis Technologies, Inc.) was injected subcutaneously proximal to the injury site at least 5 minutes before imaging. At the end of the studies, the animals were euthanized and tissue biopsies from the treated wound and the contralateral (control) wound were collected, and processed for immunohistochemistry, as described above.

Statistical analysis

The statistical significance of differences between experimental groups and/or measures was assessed using one-way, two-way, or two-way repeated-measures ANOVA followed by post-hoc multiple comparisons using the Bonferroni or Tukey method. Two-way ANOVA with one within-subjects factor (cell type) and one between-subjects factor (genotype; n = 3

animals each, values were averages across three technical replicates) were used for flow cytometry data. Two-way ANOVA with treatment type or dosage as a between-subjects factor (n = 5–30 animals per condition, pooled within genotype across experimental replicates as available) and time point as a within-subjects factor were used for the analysis of timed *in vivo* wound healing studies. Histological evaluations of scar quality were analyzed using either one-way ANOVA with treatment as the main factor, or two-way ANOVA with treatment as a between-subjects factor and scoring criterion as within-subjects factor. Immunohistochemistry data (n = 3–11 images from independent tissue sections collected from 3–5 animals per condition) were analyzed using two-way ANOVA with one between-subjects factor (treatment) and one within-subjects factor (time point, region, or marker), two-way ANOVA with two between-subjects factors (treatment-region combination and time point), or Holm-Sidak method with alpha = 0.05 and without assuming a consistent SD. All reported descriptive statistics are estimated marginal means ± standard error of the mean (SEM). All statistical analyses were conducted using GraphPad Prism 7 (GraphPad Software, Inc.).

Study approval

All animal procedures were performed following the Public Health Service Policy on Humane Care of Laboratory Animals and approved by the Institutional Animal Care and Use Committee of Massachusetts General Hospital. All efforts were made to reduce the number of animals used and to minimize animal suffering.

RESULTS

Characterization of B cells isolated from the spleen of wild-type (WT) and diabetic (*db/db*) animals

After negative immunomagnetic selection, the majority of the isolated cells (85–92%) were CD45R/B220$^+$/CD19$^+$ B cells. Erythrocytes represented the major contaminant in all samples, constituting 10–25% of isolated cells. Other cell types represented minor contaminants, comprising less than 1% of the cell isolate. Results indicated very similar profiles between the isolates from WT and *db/db* mice ($F_{(6, 24)} = 0.793$, $p = 0.584$; Fig. S1, Table S1). Further characterization showed that the majority (96.4 ± 0.73%) of the B cells in the isolate were mature naïve IgM$^+$/IgD$^+$ B cells. The composition and the relative proportions of B cell subpopulations did not differ significantly between genotypes ($F_{(1,4)} = 1.25$, $p = 0.326$; Fig. S1, Table S2).

A single topical application of enriched mature naïve B cells significantly accelerates wound closure after acute injury in WT and *db/db* animals

To determine the optimal dosage of B cells for application onto wounds, a dose response study was performed in WT mice using 0.1×10^6, 0.5×10^6, 1.5×10^6, 5×10^6, or 10×10^6 B cells per 20 mm^2 wound (Fig. S2). An application of 1.5×10^6 B cells was selected as the lowest dosage that showed a significant acceleration of wound closure ($F_{(72, 400)} = 2.92$, $p < 0.0001$). To examine the effect of B cell treatment on acute wounds, 1.5×10^6 negatively-selected B cells, T cells, or only saline were applied onto splinted full-thickness excision lesions immediately after injury. Purified HSCs at a dosage equivalent to the maximum

estimated numbers of HSC contamination in negatively selected B cell isolates (0.8%) were included as an additional control in diabetic animals. In WT animals, B-cell-treated wounds closed 2–3 days earlier than either saline or T-cell-treated controls, showing significantly reduced open wound areas after day 2 post-injury ($F_{(16, 360)} = 4.747$, $p < 0.0001$). No significant differences were observed between the saline control and the T cell treatment (Fig. 1A–B). All wounds eventually closed fully within the observed time interval, with the visible scar size being significantly smaller in B cell-treated wounds (Fig. 2F). In diabetic animals, the regenerative effect of B cells was more pronounced, with B-cell-treated wounds closing 5–6 days earlier than either saline-treated, HSC-treated or T-cell-treated controls, and showing significantly reduced areas after day 6 post-injury ($F_{(52, 780)} = 9.184$, $p < 0.0001$). B cells isolated from healthy or diabetic animals performed equally well (Fig. 1C). Notably, approximately 64% of the 50 wounds treated with saline, HSCs, or T cells progressed towards a chronic ulcer phenotype, remaining >50% open up to day 34 post-injury, with only 0.5% of the ulcers fully closed. By contrast, only 7.9% of the 38 B-cell-treated wounds remained >40% open by this time point, with 50% percent of the wounds fully closed (Fig. 1C–D).

We hypothesized that the pro-regenerative effects of B cell application are cell-mediated, and not simply based on the immediate action of molecular factors contained within the cells. To test this hypothesis, wounds were treated either with whole B cells in suspension, or with an equivalent number of B cells that were first disrupted through sonication. Live B cell treatment accelerated wound closure by approximately 3 days ($F_{(16, 136)} = 3.446$, $p < 0.0001$), performing significantly better than either equivalent numbers of lysed B cells, or saline control (Fig. 1E–F).

B cell treatment improves the quality of tissue repair

At the end of the wound healing time course, the wounded areas were excised and evaluated histologically for indicators of tissue regeneration, including overall width and thickness of the scar tissue, collagen deposition and maturation, angiogenesis, and nerve growth (see Table S3 for parameters and scoring system). In WT animals, acute B cell treatment was associated with better tissue regeneration and a smaller scar surface (Fig. 2). B-cell-treated wounds scored significantly better than wounds treated with saline or T cells ($F_{(2, 55)} = 18.34$, $p < 0.0001$). This benefit was largely due to improved patterning of collagen deposition, with fibers distributed in a reticulated pattern resembling the structure found in intact skin, enhanced angiogenesis, and significantly reduced scar width ($F_{(14, 385)} = 2.238$, $p < 0.01$; Fig. 2E). The latter measure corroborated data from area measurements of the visible scar at day 16 post injury, indicating a significantly smaller area of the scars in wounds that had been treated with B cells ($F_{(2, 45)} = 21.37$, $p < 0.0001$; Fig. 2F).

In *db/db* mice, treatment with B cells derived from the spleen of either WT or diabetic syngeneic animals led to reduced scar area and more compact scar tissue, with less vacuolization and inflammatory cell infiltration (Fig. 3). Wounds treated with either WT or *db/db* B cells scored significantly better than wounds treated with saline or T cells ($F_{(3, 62)} = 12.42$, $p < 0.0001$). This improvement was supported by the deposition and maturation of collagen fibers, enhanced angiogenesis and neuroregeneration, defined as the growth of new

nerve endings under and into the scar tissue, and significantly reduced scar width ($F_{(21, 434)} = 4.353$, $p < 0.0001$; Fig. 3F). As in WT animals, collagen fibers were deposited in a reticulated pattern in the scars of wounds treated with B cells as compared to large parallel bundles observed in controls, particularly after treatment with WT B cells (Fig. 3C'-D'). Area measurements of the visible scar or open wound at day 34 post injury showed significantly lower values in wounds that had been treated with WT or *db/db* B cells ($F_{(3, 91)} = 10.32$, $p < 0.0001$; Fig. 3G).

B cell treatment reactivates proliferative healing in chronic diabetic skin ulcers

To assess whether B cell application can re-initiate healing in a chronic ulcer, wounds were generated on the dorsal skin in obese diabetic mice and treated with saline dressing only. After 10 days all wounds were still open, and most showed rounded, non-proliferative edges typical of chronic ulcers[15]. At this time-point, the wounds were treated with WT-derived B cells or saline. A rapid reduction of over 50% in the area of the open wound was observed 4 days after B cell application (Fig. 4), and the treated wounds maintained a significant advantage in the closure rate up to 30 days ($F_{(6, 174)} = 15.97$, $p < 0.0001$). Over the course of the study, 43% of the wounds treated with B cells closed fully, as compared to only 5% of the saline treated wounds. At 30 days post injury, wounds with at least 50% of the initial surface still open were subjected to a second application of either B cells or saline control (Fig. 4C). B cell treatment again showed a positive effect as compared to saline ($F_{(1, 13)} = 6.435$, $p < 0.05$), with a 10% reduction in the open area of the treated wounds. This effect was most pronounced at 4 days post B cell application and was maintained at 8 days ($F_{(2, 26)} = 3.889$, $p < 0.05$). B cell application enhanced cell proliferation and migration in the edges of the treated wounds, as indicated by the change in the wound edge morphology from rounded to flat, forming an epithelial tongue which extended towards the wound bed (Fig. 4B, D).

B cells derived from aged *db/db* mice can accelerate wound healing in aged diabetic animals

To assess the efficacy of B cells that were subjected to prolonged exposure to a diabetic hyperglycemic environment, cells were isolated from aged (15-months-old) obese *db/db* mice and applied onto acute wounds in 6–15-month-old obese *db/db* mice. Results indicated that the B cell treatment prevented the initial inflammatory enlargement of the wounds often observed in saline-treated controls, and furthermore led to a significant acceleration of wound closure ($F_{(7, 84)} = 21.45$, $p < 0.0001$) and reduced scar size in all animals examined ($n = 7$; Fig. 4G–H).

Exogenous B cells localize to the wound bed and remain viable up to 2 weeks after application

To examine whether exogenously applied B cells are retained within or migrate away from the site of application, B cells were labeled with ^{89}Zr-protamine-conjugated Feraheme nanoparticles before application onto wound beds. Positron emission tomography combined with computed tomography (PET/CT) scanning of the whole body, showed that the signal remained well-localized within the wound bed up to 13 days (Fig. 5). Some loss of signal at the wound site may occur due to cell death and subsequent diffusion of released

nanoparticles. Indeed, when free nanoparticles were applied to the wound bed in the absence of B cells, diffusion of the signal occurred rapidly, leading to an apparent loss of signal intensity at the injury site and increased activity in other organs, including lymph nodes and spleen, by day 14 post application (Fig. 5A–C).

To examine *in situ* survival of the introduced cells, luciferase-expressing B cells were applied onto the wound bed and the mice were imaged over 24 days. Light emission indicating active enzymatic activity within the applied cells strongly declined after day 6, and reached undetectable levels by day 14 (Fig. 5D–E). These results indicate that the exogenous B cells have a limited life span of up to 2 weeks *in situ* within the wound bed.

Immunohistochemical analysis of tissue sections collected from the wound site confirmed that the number of $B220^+$ B cells in the wound bed and edges was significantly elevated after exogenous application ($F_{(1, 58)} = 37.31$, $p < 0.0001$). The introduced B cells became well integrated into the newly-formed granulation tissue (Fig. S3A–B). $B220^+$ cells were detected in significantly higher numbers in B-cell-treated wounds as compared to saline-treated controls at 1 and 4 days post application ($F_{(3, 58)} = 7.987$, $p < 0.001$), but this difference was no longer statistically significant at 17 days ($p = 0.353$; Fig. S3C).

B cell application is associated with increased fibroblast proliferation, reduced apoptosis in the wound bed and edges and a pro-regenerative wound molecular microenvironment

To examine the mechanism for the accelerated wound healing observed following B cell application, treated and control biopsies collected at 24 hours and 4 days after injury and treatment, were labeled against cleaved caspase-3 and Ki67, as markers of apoptosis or cell proliferation, respectively. Counts were normalized to the overall cell density based on DAPI counterstaining. Results showed a significant decrease in the relative numbers of apoptotic cells in wounds treated with B cells at the time of injury ($F_{(1, 48)} = 15.67$, $p < 0.001$; Fig. 6A–C, G). At the same time points, cell proliferation was significantly increased in B-cell-treated tissues as compared to saline controls ($F_{(1, 48)} = 23.59$, $p < 0.0001$; Fig. 6D–F, H).

When distinct regions of the wound were analyzed independently 4 days after injury and treatment, high numbers of B cells were associated with increased cell proliferation and reduced apoptosis, in particular in the wound bed and edges (Fig. 7B). In agreement with results indicating limited persistence of exogenous cells at the wound site, proliferating $Ki67^+B220^+$ B cells were never observed *in situ* (Fig. 7A, C). Virtually all mitotic cells were fibroblasts, identified by immunolabeling with a monoclonal antibody raised against mouse fibroblasts, and they were localized proximally to the B cells (Fig. 7A, D). These results indicate that the B cell-mediated acceleration of wound healing is associated with a skewing of the apoptosis-cell proliferation balance in the wound bed and edges, leading to a net addition of cells.

B cell treatment was associated with multiple changes in the molecular microenvironment of the wound bed. At 4 days after injury, a significant increase in TGF-β was observed in cells of the granulation tissue in B cell-treated wounds ($F_{(2, 26)} = 7.783$, $p < 0.01$; Fig. S4A–B). No significant changes in expression were observed for other growth factors such as FGF2, or in the anti-inflammatory cytokine IL-10 at this time point (Fig. S4E). Conversely, a

significant decrease in the expression of MMP2, a major proteolytic enzyme, within and around the cells in the wound bed was observed in B cell-treated wounds as compared to saline controls ($F_{(1, 18)} = 45.97$, $p < 0.001$; Fig. S4C–D). No significant change was observed in the expression of MMP8 between B cell treated and control wounds (Fig. S4F). These results further support the view that the application of B cells induces discrete changes in the wound microenvironment that accelerate wound closure.

B cell application accelerates the dynamics of neutrophil infiltration into the wound

To examine the dynamics of inflammatory cell infiltration at the wound site, as related to B cell application, tissue sections from wound biopsies collected at 24 hours, 4 days, 10 days, and 16 days after injury were stained with hematoxylin and eosin and the numbers of neutrophils were analyzed in the wound bed, wound edge and the periphery of the wound biopsy (Fig. S5). Baseline numbers of neutrophils in the intact skin as well as distally to the wound were very low at 1.1×10^6 and 1.6×10^6 cells/μm^3 (Fig. S5A). In wounds treated with B cells, significantly increased numbers of neutrophils were observed in the wound bed at early time points, particularly at 24 hours when they reached 45 ($\pm$ 1.1)$\times10^6$ cells/μm^3 as compared to 29 ($\pm$ 2.8)$\times10^6$ cells/μm^3 ($p < 0.0001$) in saline-treated controls and, somewhat less pronounced, at 4 days after the injury, decreasing rapidly at later time points. By contrast, saline-treated controls showed less acute neutrophil infiltration early after injury, but the rate of reduction in neutrophil numbers over time was 2.5 times slower than in B cell-treated wounds, as indicated by the linear regression slope (Fig. S5B). By 10 days post injury, the difference in neutrophil numbers reversed, with saline-treated wounds having on average 19 ($\pm$ 1.8)$\times10^6$ cells/μm^3 while B cells treated wounds showed only 11 ($\pm$ 3)$\times10^6$ cells/μm^3. Moreover, in the wound edge, the peak of neutrophil infiltration was observed at 1 day in B cell treated wounds with 19 ($\pm$ 2.6)$\times10^6$ cells/μm^3, but at 10 days in saline-treated controls with 11.5 ($\pm$ 1.9)$\times10^6$ cells/μm^3. These results suggest an overall acceleration of the acute response to injury in animals treated with B cells.

B cell treatment enhances regeneration of vasculature and nerve fibers in the scar tissue

To investigate whether B cell application alters the trophic environment of the wound and affects long-term regenerative phenomena, including angiogenesis and neuroregeneration, tissue sections collected from healed scar tissue that had been treated with either B cells or saline were labeled with anti-CD31 and anti-β-III tubulin antibodies to visualize endothelial cells and neurites, respectively (Fig. 8). Quantification of the area covered by immunolabeling with either of these markers showed that the acute B cell application was associated with significant increases in the extent of angiogenesis and neuroregeneration within the scar tissue at day 16 post-injury, as compared to saline-treated controls ($F_{(1, 17)} = 20.66$, $p < 0.001$; Fig. 8C). These results confirm a broad-impact pro-regenerative effect of exogenous B cells, which appears to lead to a shift in the trophic properties of the wound microenvironment, even at long intervals after injury.

Moreover, nerve endings that grew under and within the scar tissue of wounds that were treated with B cells at the time of injury showed significantly increased expression of growth-associated protein 43 (GAP43), an established marker of axonal regeneration[16] (Fig. S6). Regenerating nerve endings were not immunopositive for the neuropeptide substance P,

and thus were not peptidergic C fibers[17], suggesting that the enhanced neurite growth was likely not associated with detrimental increases in nociceptive sensitivity in the scar tissue (Fig. S6).

DISCUSSION

This study demonstrates for the first time, to our knowledge, that the progression of wound healing in the skin can be positively manipulated by altering the balance of a mature immune cell population, specifically B cells, within the wound microenvironment. While the roles of neutrophils and macrophages in wound healing are well-documented, little is known regarding B cells in this context. Some studies report that no B cells can be found at the site of a lesion[18], while others describe only very low cell numbers infiltrating the wound bed[10]. In the present study, B cells were detected at above-baseline levels at 4 days after injury in saline-treated control wounds, and persisted at that level up to 17 days post injury in WT mice. These results are in agreement with other reports demonstrating the presence of B cells in the wound bed at 3 and 7 days after a skin lesion[11], and indicate that B cells do normally infiltrate the wound tissue, albeit in low numbers. Direct application of exogenous B cells shifted the proportion of this lymphocyte population present in the wound bed, and the time after the injury when they become locally abundant.

While no previous study has examined the impact of direct B cell transfer into the wound environment, several studies indicate that circulating B cells play an active role in wound healing[10]. It has been hypothesized that B cell production of IgG1 immunoglobulins aids in the opsonization of dead cells at the injury site, facilitating their clearance by macrophages[10]. Mice deficient in the B cell-specific marker CD19 show impaired wound healing, while overexpression of CD19 on B cells accelerates wound closure[11]. Interestingly, ECM components can induce CD19-dependent TLR signaling in the B cells localized in the wound, which in turn induces the expression of key cytokines such as IL-6, IL-10, and TGF-β[11]. These factors can directly reduce inflammation and promote the proliferation of fibroblasts and keratinocytes, for example through the TGF-β pathway[19], but they can also act indirectly, by regulating skin expression of cytokines and growth factors. Indeed, in the present study, the application of B cells onto acute wounds led to an initial increase in the numbers of neutrophils infiltrating into the wound bed, followed by a rapid decrease. The rate of neutrophil depletion in the granulation tissue of the wound bed was 2.5-fold faster than in saline-treated controls, supporting the hypothesis of an overall acceleration in the timeline of wound healing stages. Interestingly, in $CD19^{-/-}$ knockout mice, both reduced neutrophil infiltration as well as delayed wound healing have been reported[11].

An investigation that used direct exogenous application of isolated B lymphocytes at the site of cardiac ischemia showed that intramyocardial injection of B cells into injured myocardium preserved cardiac function by preventing cardiomyocyte apoptosis and stimulating local cell proliferation [9]. These results are consistent with the findings of the present study, where B cell application to the wound bed at the time of the lesion was associated with significantly reduced apoptosis and enhanced fibroblast proliferation at 1 and 4 days after injury and treatment. This effect of B cells may be mediated via β-catenin,

an important regulator of fibroblast behavior during the proliferative phase of dermal wound repair[19].

The results of the present study point to a complex multi-modal modulatory effect of exogenously added B cells in the context of wound healing. In granulation tissue at 4 days post injury, B cell treatment was associated with an increase in the expression of major activating growth factors such as TGF-β, which at this stage is observed predominantly in fibroblasts and wound macrophages. At the same time, the expression of MMP2, a protease whose up-regulation is an indicator of chronic wounds[20], was reduced in B cell treated wounds as compared to saline controls. Together, these observations support the notion that the presence of B cells can reduce the proteolytic characteristics of the wound microenvironment, preventing tissue degradation, and at the same time can promote a shift towards a more trophic milieu that can enhance fibroblast proliferation in the granulation tissue.

Application of B cells at the time of injury in the present study was associated with a significant increase in the number of capillaries and nerve endings within the area of the scar over two weeks later. During wound healing, angiogenic capillary sprouts invade the fibrin/fibronectin-rich wound clot and organize into a microvascular network throughout the granulation tissue[21]. Neutrophils infiltrating at early stages of wound healing have been previously shown to promote angiogenesis[22], making the significantly increased neutrophil infiltration at the wound site observed at early time points in B cell-treated wounds a potential indirect mechanism for increased vascularization. Moreover, while B cells are known to secrete some proangiogenic factors upon stimulation, such as TGF-β[11], they likely support angiogenesis indirectly, by inducing the secretion of cytokines and growth factors in neighboring fibroblasts and keratinocytes, as observed in the wound bed. Similarly, B cell therapy creates a permissive microenvironment for nerve fiber regrowth. Histological analysis showed that in WT mice, approximately 64% of the wounds (9/14) treated acutely with B cells showed pronounced innervation and cutaneous nerve growth under the scar tissue at 16 days post injury, as compared to only 20% of the wounds (6/30) treated with saline. Interestingly, the converse effect is well documented, as denervation of a skin domain slows the rate of wound healing in that area by reducing the inflammatory infiltrate, including T and B lymphocytes[23]. These results point to a significant reciprocal neuroimmune crosstalk in the wound microenvironment as observed in lymphoid organs [24], which could be used as a mechanism for regulating neuroregeneration in the context of injury [25]. Such an effect will be especially relevant for the treatment of diabetic wounds and ulcers, where main obstacles to healing include vasculopathy and neuropathy[1], [26]. Importantly, B cells isolated from aged diabetic mice, and applied onto wounds in aged *db/db* mice, all of which showed pronounced hyperglycemia, still showed unaltered capacity for promoting wound healing, providing a promising option for the development of autologous immunotherapies for patients with diabetes.

In summary, we demonstrate that the topical application of mature, minimally-manipulated B lymphocytes can alter the progression of acute and chronic wounds in a spatio-temporally localized manner. Taken together, these data support the view that the experimental manipulation of the numbers and the timing of B cells arriving at the wound site affects

multiple aspects of the inflammatory and proliferative stages of wound healing, modulating and abbreviating the inflammatory phase and inducing a pro-regenerative molecular milieu in the wound bed. These results support the further development of a novel and promising autologous B cell-based immunotherapy that may be applicable to the treatment of difficult to treat acute and chronic wounds including most notably, diabetic foot ulcers.

Supplementary Material

Refer to Web version on PubMed Central for supplementary material.

Acknowledgments

We are grateful to Paul Papagni, J.D. and Dr. Alexander Justicz, MD from Holy Cross Hospital for guidance and helpful suggestions on the studies. The authors would like to thank Drs. Patrick M. Reeves, Ph.D. and Shaw H. Warren, MD for helpful suggestions and comments on the manuscript, and Drs. Khalid Shah, Ph.D. and Jasneet K. Khalsa, Ph.D. for the generous gift of fLuc-eGFP B cells. This research was supported by the Specialized Histopathology Services Core Facility of the Dana-Farber/Harvard Cancer Center (P30 CA06516). Background Intellectual Property required for performing the research plan was provided by Innovations at Massachusetts General Hospital and Holy Cross Hospital.

Sources of Funding: Funding for these studies was provided through the Trinity Innovation Fund by Holy Cross Hospital, Ft. Lauderdale, Florida, USA, the VIC Innovation Fund, and NIH grant 5R01EB017699-03 to CK. Dr. Orgill receives research support from the Gillian Reny Stepping Strong Fund.

LIST OF ABBREVIATIONS

Ig	immunoglobulin
ECM	extracellular matrix
CD	cluster of differentiation
TLR-4	toll-like receptor 4
TGF-β	transforming growth factor beta
IL	interleukin
HSCs	hematopoietic stem cells
WT	wild-type
ANOVA	analysis of variance
Zr	zirconium
PET/CT	positron emission tomography combined with computed tomography
MIP	maximum intensity projection
CPM	counts per minute
DAPI	4’,6-diamidino-2-phenylindole
GAP43	growth-associated protein 43

FBS	fetal bovine serum
EDTA	ethylenediaminetetraacetic acid
PBS	phosphate-buffered saline
TBS	Tris-buffered saline

References

1. Sen CK, Gordillo GM, Roy S, Kirsner R, Lambert L, Hunt TK, et al. Human skin wounds: a major and snowballing threat to public health and the economy. Wound Repair Regen. 2009; 17(6):763–71. [PubMed: 19903300]
2. Garwood CS, Steinberg JS. What's new in wound treatment: a critical appraisal. Diabetes Metab Res Rev. 2016; 32(Suppl 1):268–74.
3. Trøstrup H, Bjarnsholt T, Kirketerp-Møller K, Høiby N, Moser C. What Is New in the Understanding of Non Healing Wounds Epidemiology, Pathophysiology, and Therapies. Ulcers. 2013; 2013:8.
4. Park JE, Barbul A. Understanding the role of immune regulation in wound healing. Am J Surg. 2004; 187(5A):11S–6S. [PubMed: 15147986]
5. Stadelmann WK, Digenis AG, Tobin GR. Physiology and healing dynamics of chronic cutaneous wounds. Am J Surg. 1998; 176(2A Suppl):26S–38S. [PubMed: 9777970]
6. Trengove NJ, Stacey MC, MacAuley S, Bennett N, Gibson J, Burslem F, et al. Analysis of the acute and chronic wound environments: the role of proteases and their inhibitors. Wound Repair Regen. 1999; 7(6):442–52. [PubMed: 10633003]
7. Hoffman W, Lakkis FG, Chalasani G. B Cells, Antibodies, and More. Clin J Am Soc Nephrol. 2016; 11(1):137–54. [PubMed: 26700440]
8. Li R, Rezk A, Healy LM, Muirhead G, Prat A, Gommerman JL, et al. Cytokine-Defined B Cell Responses as Therapeutic Targets in Multiple Sclerosis. Front Immunol. 2015; 6:626. [PubMed: 26779181]
9. Goodchild TT, Robinson KA, Pang W, Tondato F, Cui J, Arrington J, et al. Bone marrow-derived B cells preserve ventricular function after acute myocardial infarction. JACC Cardiovasc Interv. 2009; 2(10):1005–16. [PubMed: 19850263]
10. Nishio N, Ito S, Suzuki H, Isobe K. Antibodies to wounded tissue enhance cutaneous wound healing. Immunology. 2009; 128(3):369–80. [PubMed: 20067537]
11. Iwata Y, Yoshizaki A, Komura K, Shimizu K, Ogawa F, Hara T, et al. CD19, a response regulator of B lymphocytes, regulates wound healing through hyaluronan-induced TLR4 signaling. Am J Pathol. 2009; 175(2):649–60. [PubMed: 19574428]
12. Könnecke I, Serra A, El Khassawna T, Schlundt C, Schell H, Hauser A, et al. T and B cells participate in bone repair by infiltrating the fracture callus in a two-wave fashion. Bone. 2014; 64:155–65. [PubMed: 24721700]
13. Wang X, Ge J, Tredget EE, Wu Y. The mouse excisional wound splinting model, including applications for stem cell transplantation. Nat Protoc. 2013; 8(2):302–9. [PubMed: 23329003]
14. Yuan H, Wilks MQ, El Fakhri G, Normandin MD, Kaittanis C, Josephson L. Heat-induced-radiolabeling and click chemistry: A powerful combination for generating multifunctional nanomaterials. PLoS One. 2017; 12(2):e0172722. [PubMed: 28225818]
15. Brem H, Tomic-Canic M. Cellular and molecular basis of wound healing in diabetes. J Clin Invest. 2007; 117(5):1219–22. [PubMed: 17476353]
16. Grasselli G, Strata P. Structural plasticity of climbing fibers and the growth-associated protein GAP-43. Front Neural Circuits. 2013; 7:25. [PubMed: 23441024]
17. Steinhoff MS, von Mentzer B, Geppetti P, Pothoulakis C, Bunnett NW. Tachykinins and their receptors: contributions to physiological control and the mechanisms of disease. Physiol Rev. 2014; 94(1):265–301. [PubMed: 24382888]

18. Martin CW, Muir IF. The role of lymphocytes in wound healing. Br J Plast Surg. 1990; 43(6):655–62. [PubMed: 2257414]
19. Bielefeld KA, Amini-Nik S, Alman BA. Cutaneous wound healing: recruiting developmental pathways for regeneration. Cell Mol Life Sci. 2013; 70(12):2059–81. [PubMed: 23052205]
20. Martins VL, Caley M, O'Toole EA. Matrix metalloproteinases and epidermal wound repair. Cell Tissue Res. 2013; 351:255–68. [PubMed: 22526628]
21. Tonnesen MG, Feng X, Clark RA. Angiogenesis in wound healing. J Investig Dermatol Symp Proc. 2000; 5(1):40–6.
22. Zhang Y, Li L, Liu Y, Liu ZR. PKM2 released by neutrophils at wound site facilitates early wound healing by promoting angiogenesis. Wound Repair Regen. 2016; 24(2):328–36. [PubMed: 26808610]
23. Richards AM, Floyd DC, Terenghi G, McGrouther DA. Cellular changes in denervated tissue during wound healing in a rat model. Br J Dermatol. 1999; 140(6):1093–9. [PubMed: 10354076]
24. Jung WC, Levesque JP, Ruitenberg MJ. It takes nerve to fight back: The significance of neural innervation of the bone marrow and spleen for immune function. Semin Cell Dev Biol. 2016
25. Klebe D, McBride D, Flores JJ, Zhang JH, Tang J. Modulating the Immune Response Towards a Neuroregenerative Peri-injury Milieu After Cerebral Hemorrhage. J Neuroimmune Pharmacol. 2015; 10(4):576–86. [PubMed: 25946986]
26. Uccioli L, Izzo V, Meloni M, Vainieri E, Ruotolo V, Giurato L. Non-healing foot ulcers in diabetic patients: general and local interfering conditions and management options with advanced wound dressings. J Wound Care. 2015; 24(4 Suppl):35–42. [PubMed: 25853647]

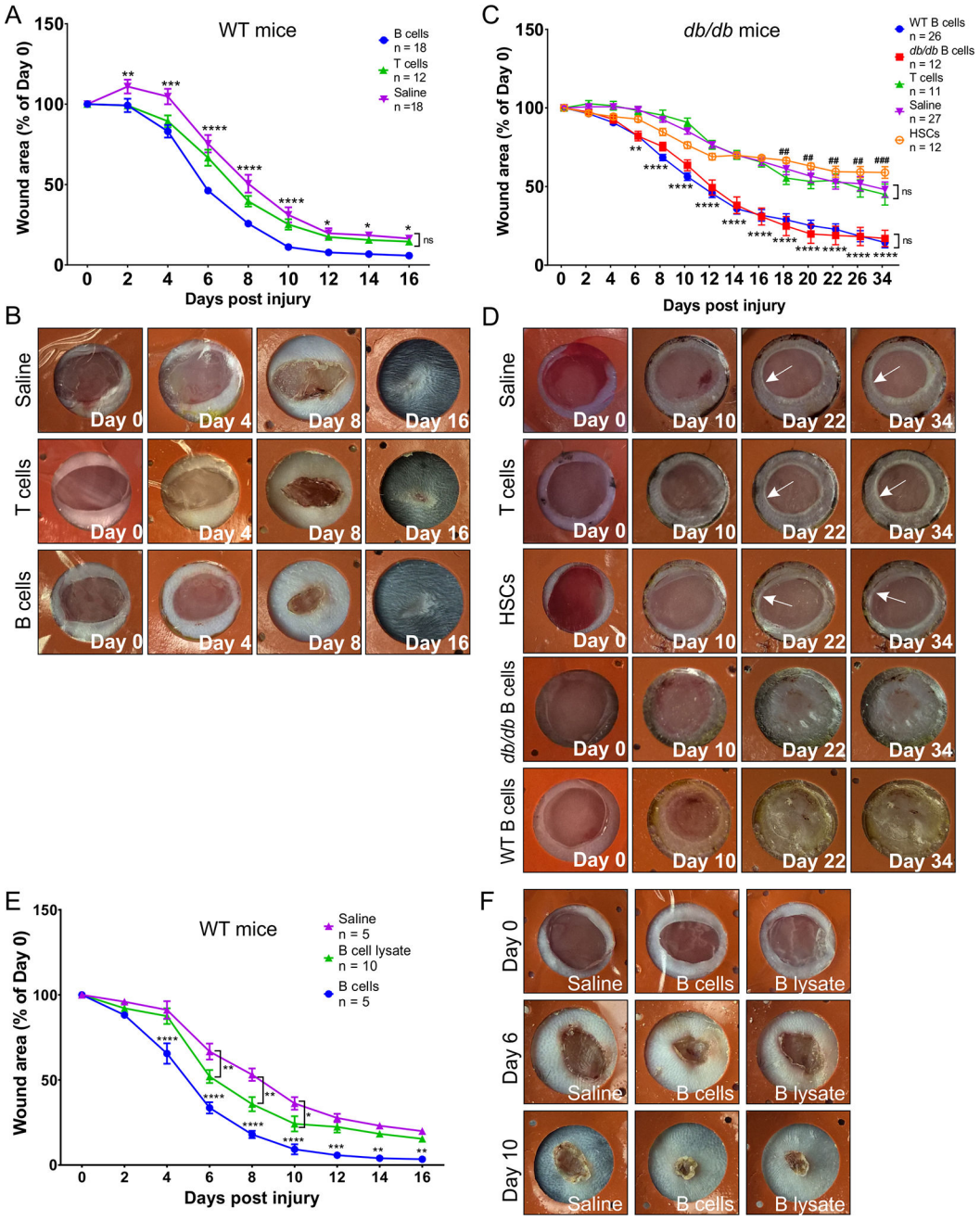

Figure 1. A single application of B cells at the time of lesion accelerates wound healing in WT and diabetic mice

A. Wound closure rate in WT animals. After lesioning and treatment application, the area of the open wound or visible scar was measured every 2 days. Wounds treated with B cells immediately after the injury showed significantly faster reduction in size and a smaller scar surface at the end point of the experiments as compared to T cell or saline treated controls. Edema and inflammation can cause an initial enlargement of the wound area, although this was mostly observed in wounds treated with saline dressing only. Data are derived from 6 independent experiments. Significance was assessed using two-way repeated-measures ANOVA followed by Tukey's multiple comparisons test. * $p < 0.05$; ** $p < 0.01$; *** $p <$

0.001; **** $p < 0.0001$. **B**. Representative examples of wound closure illustrating the effect of the B cell treatment at key time points after wound induction and treatment. Inner diameter of silicone splints = 7 mm. **C**. Wound closure rate in *db/db* animals. After lesioning and treatment application, the area of the open wound or visible scar, respectively, was measured every 2–4 days. Wounds treated with B cells isolated from either WT or diabetic mouse spleen immediately after the injury showed significantly faster reduction in size and a smaller scar surface at the end point of the experiments, with more wounds fully closed. Data are derived from 6 independent experiments. Significance was assessed using two-way repeated-measures ANOVA followed by Tukey's multiple comparisons test. ** $p < 0.01$; *** $p < 0.001$; **** $p < 0.0001$, B cells vs. all other treatments; ## $p < 0.01$; ### $p < 0.001$, HSC vs. saline. **D**. Representative examples of wound closure in diabetic animals illustrating the effect of the B cell treatment versus controls at key time points after wound induction and treatment. Full closure of the wounds was commonly observed in the B cell treated groups, while lasting chronic ulcers, showing characteristic rounded edges (arrows) were apparent in wounds treated with saline, T cells, or HSCs. **E**. Wound closure rate after lesioning and treatment of the wound with B cells homogenized through sonication shows a modest benefit as compared to saline control at intermediate time points during the wound healing time course. Wounds treated with live B cells immediately after the injury showed the expected rapid reduction in size and a smaller scar surface at the end point of the experiments. Data are derived from 2 independent experiments. Significance was assessed using two-way repeated measures ANOVA followed by Tukey's multiple comparisons test. * $p < 0.05$; ** $p < 0.01$; *** $p < 0.001$; **** $p < 0.0001$. **F**. Representative examples of wound closure illustrating the effect of the live B cell treatment as compared to cell lysate or saline at key time points after wound induction and treatment. Inner diameter of silicone splints = 7 mm.

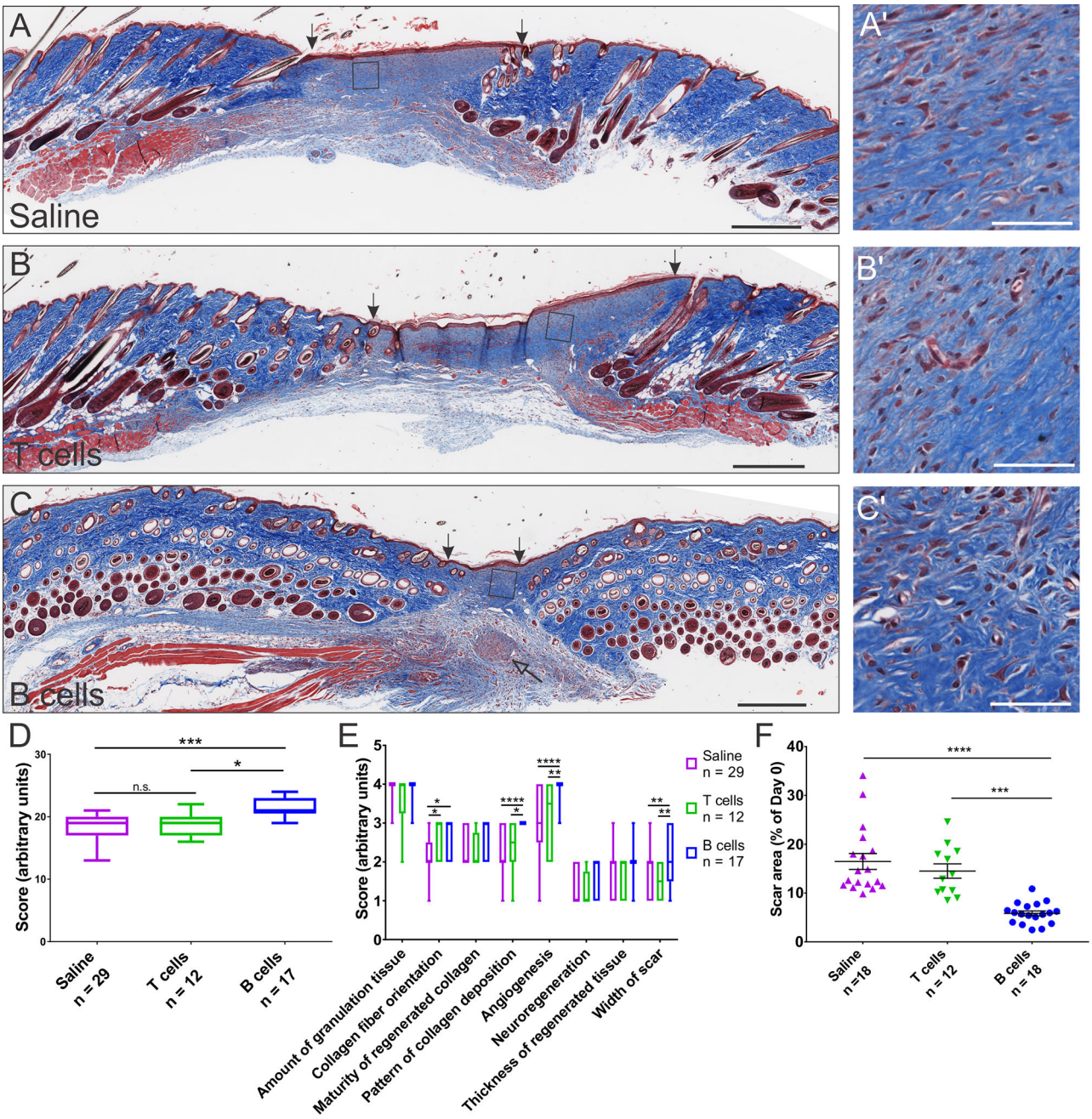

Figure 2. Wounds treated acutely with B cells show improved structural recovery in WT animals

A–C Transverse sections through the scar tissue at 16 days post-injury were stained with Masson's Trichrome, which reveals collagen deposition and maturity (blue). Scale bars, 500 μm. Areas enclosed in squares are shown at high magnification on the right (**A'–C'**). Scale bars, 50 μm. The width of the scar at this time point was significantly reduced in wounds treated with B cells at day 0 (arrows indicate the edges of the scar tissue). Nerve endings that grew under and into the scar tissue were frequently observed in the wounds treated with B cells (open arrow). **D**. Blinded scoring of the scar sections based on aggregate histological criteria showed significant advantage of wounds treated with B cells as compared to saline

or T cell controls. **E**. Detailed analysis showing individual scoring criteria indicates that the main benefits associated with the B cell treatment are derived from improved deposition of collagen fibers, increased angiogenesis, and a reduction in the width of the scar. **F**. Surface area measurements of the scar at the end point of healing experiments show a significant reduction in the area of the scar in wounds treated with B cells at day 0. Data were pooled from 6 independent experiments. Significance was assessed using one-way (**F**) or two-way repeated-measures ANOVA (**D, E**), follwed by Tukey's multiple comparisons test. * $p < 0.05$; ** $p < 0.01$; *** $p < 0.001$; **** $p < 0.0001$.

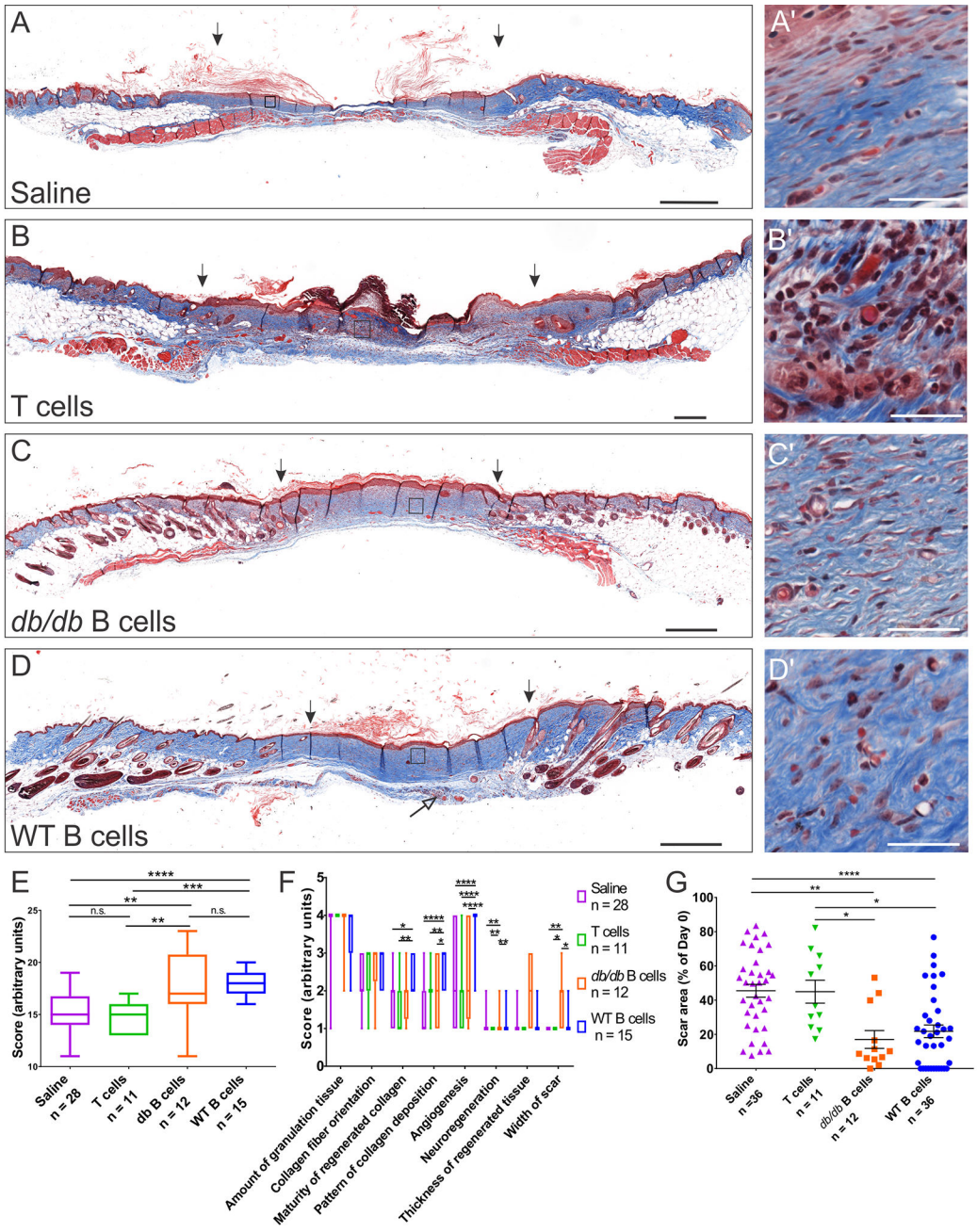

Figure 3. B cell treatment at the time of injury improves the regenerative outcome in an obese diabetic mouse model

A–D Transverse sections through the wound bed at 34 days post-injury were stained with Masson's Trichrome and evaluated for collagen deposition and maturity (blue). Scale bars, 500 μm. Areas enclosed in squares are shown at high magnification on the right (**A'–D'**). Scale bars, 40 μm. The thickness of the regenerated tissue is increased in wounds treated with B cells derived from either WT or diabetic animals, while the width of the scar at this time point was significantly reduced (arrows indicate the edges of the scar tissue). Nerve endings growing under and into the scar tissue were frequently observed in the wounds treated with B cells (**D**, open arrow). By contrast, T cell treatment led to a higher level of

immune cell infiltration at the wound site and poor wound healing, with pronounced hyperkeratosis (**B, B'**). **E**. Blinded scoring of the scar sections based on aggregate histological criteria showed a significant advantage of wounds treated with B cells derived from either WT or *db/db* animals as compared to saline or T cell controls. **F**. Analysis of individual scoring criteria indicates that the B cell treatment is associated with improved deposition and maturation of collagen fibers, increased angiogenesis and neuroregeneration as well as a reduction in the width of the scar. **G**. Scar surface measurements at the end point of healing experiments show a significant reduction in the area of the scar in wounds treated with B cells at day 0. Data were pooled from 6 independent experiments. Significance was assessed using one-way (**E, G**) or two-way ANOVA (**F**), followed by Tukey's multiple comparisons test. * $p < 0.05$; ** $p < 0.01$; *** $p < 0.001$; **** $p < 0.0001$.

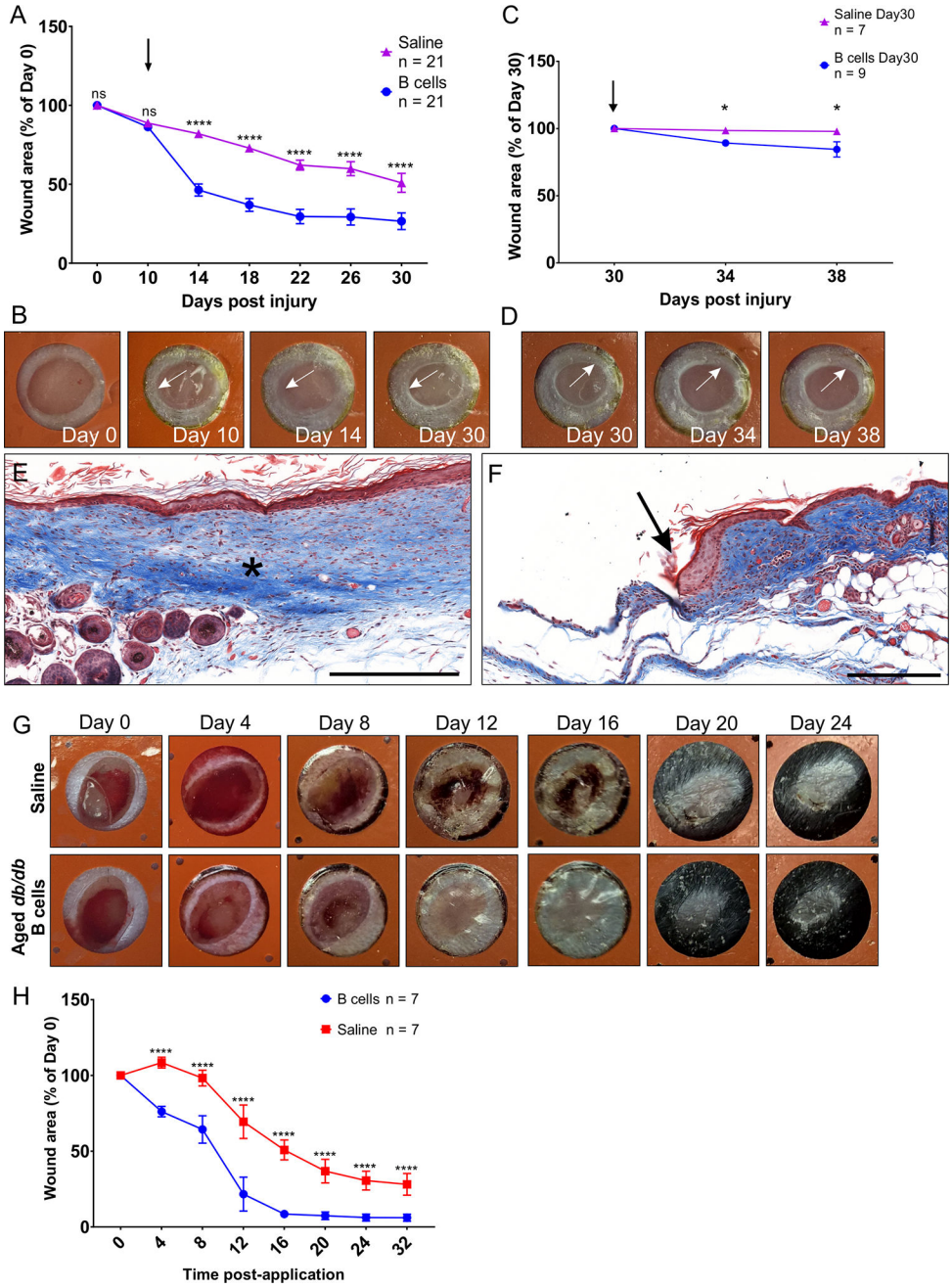

Figure 4. B cell treatment reactivates proliferative wound healing in chronic diabetic skin ulcers and in aged diabetic animals

A Wounds were treated with 2 million B cells in saline or saline control 10 days after injury (arrow), and the area of the wound was measured over 30 days. A pronounced reduction in the area of the open wound was observed in wounds treated with B cells at 4 days post application and this was maintained throughout the course of the study. Significance was assessed using two-way repeated-measures ANOVA, followed by Tukey's multiple comparisons test. **** = $p < 0.0001$; * = $p < 0.05$. **B**. Example of a wound illustrating static wound edge morphology at day 10 (arrow), which is temporarily reversed by B cell treatment at day 14, before it reverts to a static rounded-edge phenotype characteristic of

chronic ulcers by day 30. **C**. At day 30, wounds that were still open received a second application of 2 million B cells or saline control, respectively (arrow). The B cell treatment led to a small but significant reduction in open wound area 4 days later. **D**. Example of a wound illustrating the reduction in wound area correlated with a change in the morphology of the wound edge from rounded (static) at the time of application (day 30) to growing (proliferating) at day 34, before reverting to the static morphology by day 38. **E**. Transverse section through a fully healed wound at day 38. Masson's Trichrome staining shows even healing and collagen deposition at the interface between the intact skin and the scar tissue (asterisk). Scale bar, 250 μm. **F**. Transverse section through the edge of a non-healing chronic wound collected at day 38 post-injury, stained with Masson's Trichrome. Note the rounded, non-proliferative edge of the wound (arrow). Scale bar, 250 μm. **G**. Effect of B cells isolated from a 15-month old animal on wound closure in a 12-month old *db/db* mouse. Note that the rate of wound closure is accelerated and the size of the scar is visibly smaller in the wound treated with B cells as compared to saline control. **H**. Acute application of B cells isolated from 15-month old obese *db/db* animals significantly accelerated the closure of wounds in 6–15-months-old obese *db/db* mice (n = 7).

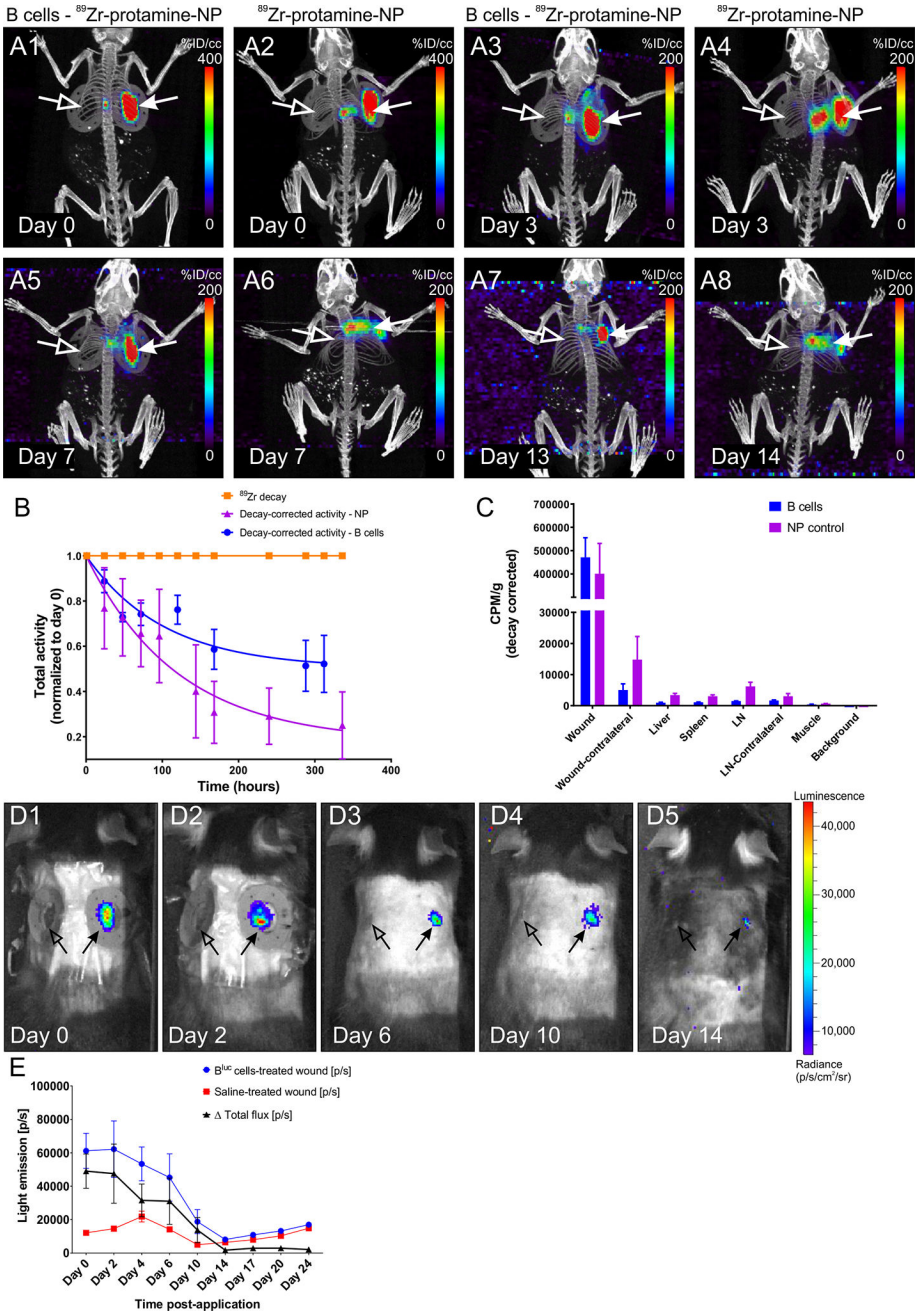

Figure 5. PET/CT tracking of B cells after application to the wound bed

A1–8 Representative maximum intensity projection (MIP) images of PET/CT scans from a WT animal at various intervals after application of ^{89}Zr-protamine-nanoparticle-labeled B cells or equal amounts of nanoparticle control. Note the highly restricted localization of the radioactive signal to the treated wound bed and edges (arrows) in the cell-treated condition (**A1, A3, A5, A7**), while substantial diffusion of the radioactivity was observed in the absence of cells (**A2, A4, A6, A8**; nanoparticle alone). Virtually no signal can be detected in the contralateral wound (open arrows) or in other organs of the body at this signal intensity. **B**. ^{89}Zr-decay-corrected radioactivity at the treated wound site (n = 4 animals per condition)

indicates that the leakage of activity from the wound site is much more pronounced if the nanoparticle is applied in the absence of cells. ^{89}Zr decay is set at 1 and shown for comparison. **C**. Gamma counter measurements of residual radioactivity at the end point of the experiments in various organs confirms the localization of the signal in the B cell treated wounds and the increased distribution to liver and lymph nodes after free nanoparticle application. CPM/g = counts per minute per gram tissue. **D1–5**. B cell survival at the wound site. Intravital imaging of a WT mouse at multiple time points after application of B^{luc} cells (right-side wound, arrow) or saline control (left-side wound, open arrow). **E**. Light emission from the wound site treated with luciferase-expressing B cells (n = 6 animals per condition) indicates that the cells survive in situ up to approximately 14 days after application, with numbers of viable cells decreasing markedly after day 6. [p/s] = photons per second.

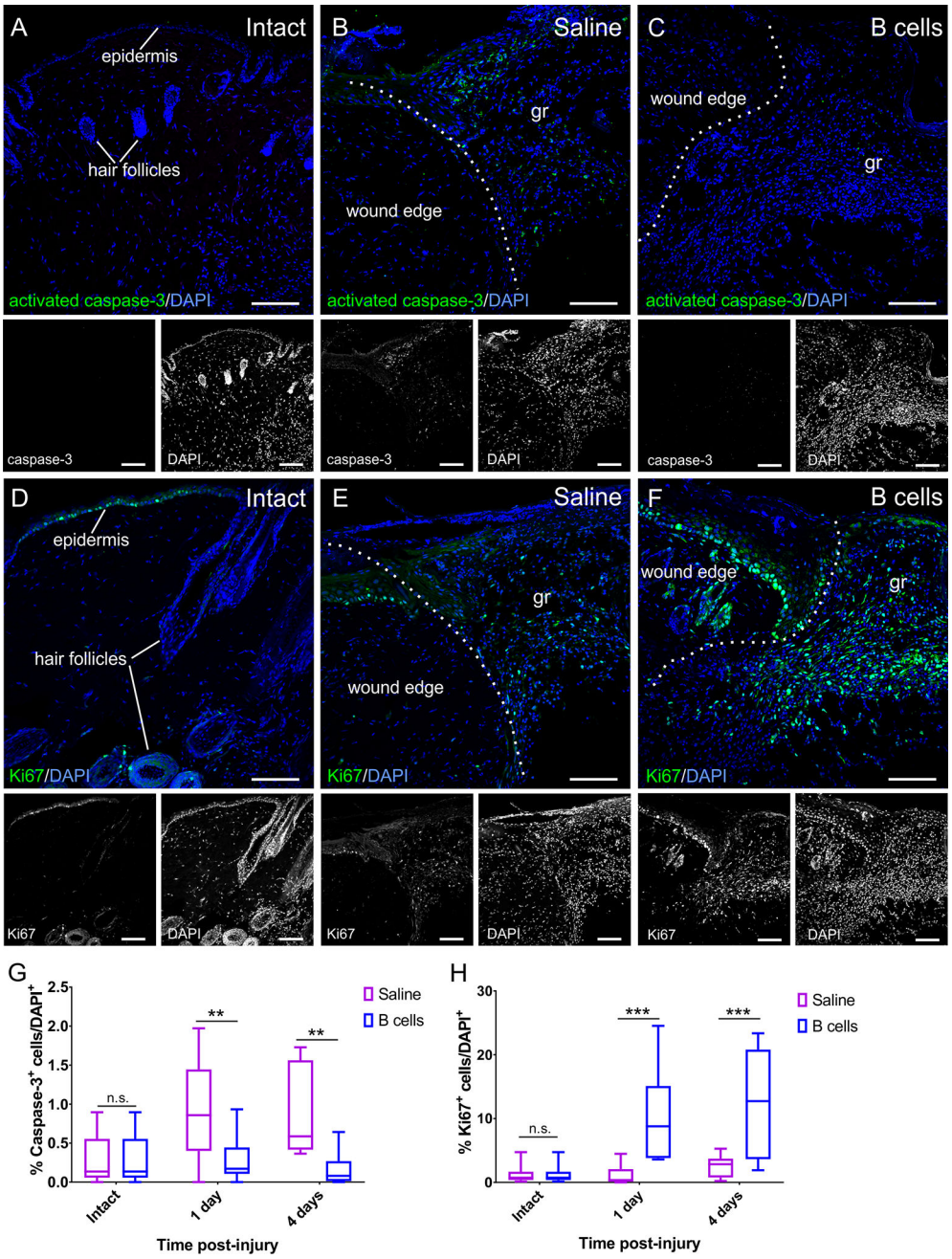

Figure 6. B cell application at the time of injury alters the rates of apoptosis and cell proliferation in the wound bed and edges

A–C Confocal images of transverse sections through the wound edge collected at 4 days post-injury are shown immunolabeled against the apoptosis marker activated caspase-3. Cell nuclei are counterstained with DAPI. While very few caspase-3-positive cells can be found in intact skin (**A**), injury induces high levels of apoptosis (**B**), which is significantly reduced in wounds treated with B cells (**C**). Scale bars, 100 μm. **D–F**. Confocal images of transverse sections through the wound edge at 4 days post-injury immunolabeled against the cell proliferation marker Ki67. Cell nuclei were counterstained with DAPI. Cell proliferation in the intact skin is mostly restricted to the stem cells in the hair follicles and the epidermis

(**D**). Injury induces a regenerative response, elevating numbers of proliferating cells which invade the wound bed (**E**), and this response appears greatly amplified in wounds treated with B cells (**F**). gr = granulation tissue in the wound bed. Scale bars, 100 μm. **G–H**. Quantitative analysis of apoptotic caspase-3-immunopositive cells (**G**) and proliferating Ki67-immunopositive cells (**H**) in the wound bed and edges at 1 and 4 days post-injury. Scale bars, 100 μm. At least 3 fields from 3 distinct sections were analyzed per animal; at least 3 animals were analyzed per condition and time point. Statistical significance was assessed by two-way ANOVA, followed by Tukey's multiple comparisons test.** = $p < 0.01$; *** = $p < 0.001$; **** = $p < 0.0001$.

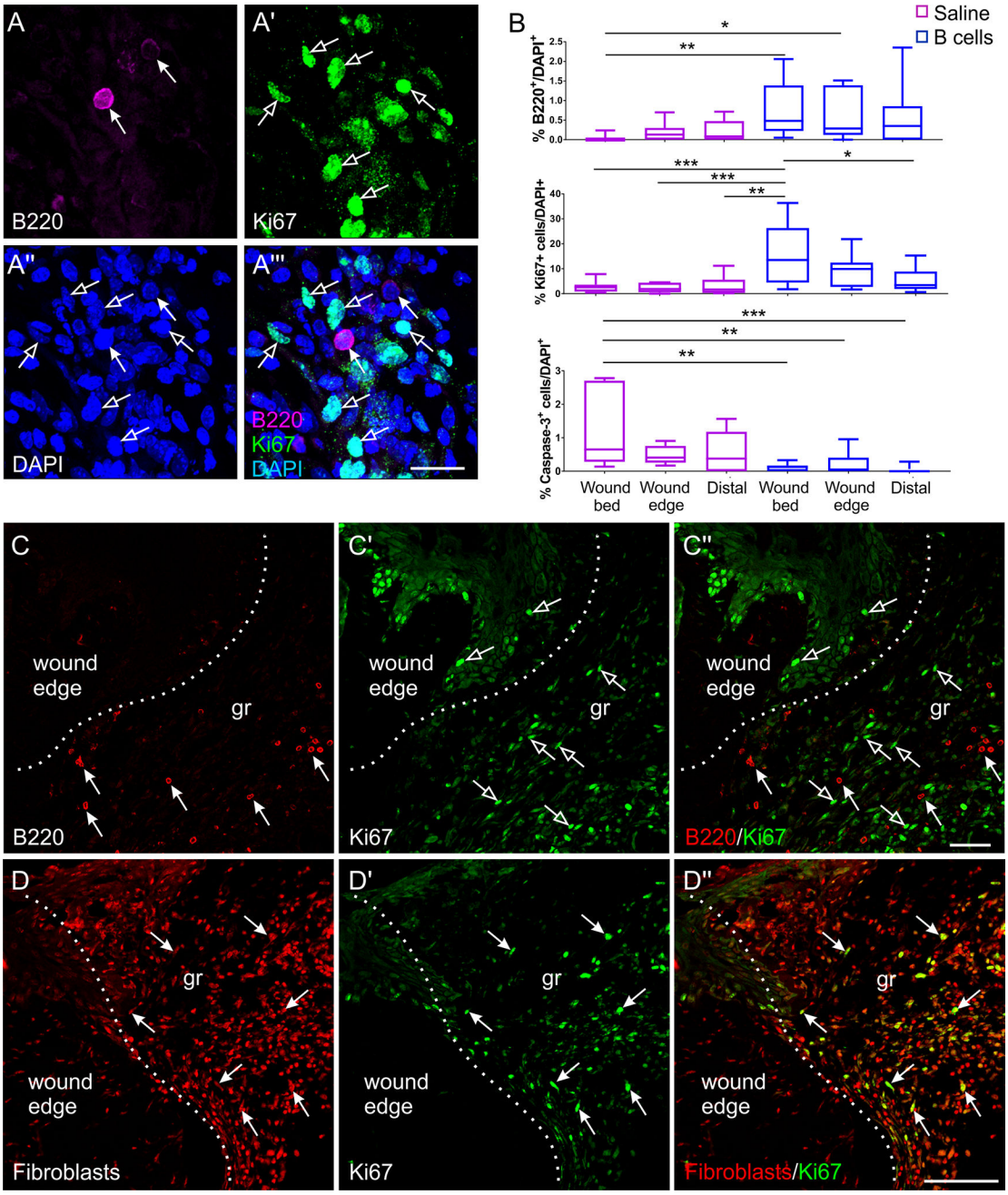

Figure 7. Cellular dynamics at the wound site after B cell application

A-A'" High-magnification confocal image of a transverse section through the wound bed showing B cells (arrows) surrounded by multiple mitotic cells (open arrows). Cell nuclei are counterstained with DAPI. Scale bar, 20 μm. **B**. Quantitative analysis of $B220^+$ B cells (top), $Ki67^+$ proliferating cells (middle), and cleaved $caspase\text{-}3^+$ apoptotic cells (bottom) in the different regions of a wound at 4 days post-injury and treatment (n = 3 animals per condition) show a correlative association between the levels of B cells present at a certain location and cell proliferation or death, respectively. Statistical significance was assessed by two-way ANOVA, followed by Tukey's multiple comparisons test. * $p < 0.05$; ** $p < 0.01$;

*** $p < 0.001$. **C-C”**. Confocal images of transverse sections through the edge of a B cell-treated wound, illustrating that while both B cells (arrows) and proliferating cells (open arrows) are present in abundance at the wound site, B cells were never observed to be proliferating. Scale bar, 50 μm. **D-D”**. Multiple immunolabeling shows that virtually all of the $Ki67^+$ proliferating cells are fibroblasts. Scale bar, 100 μm.

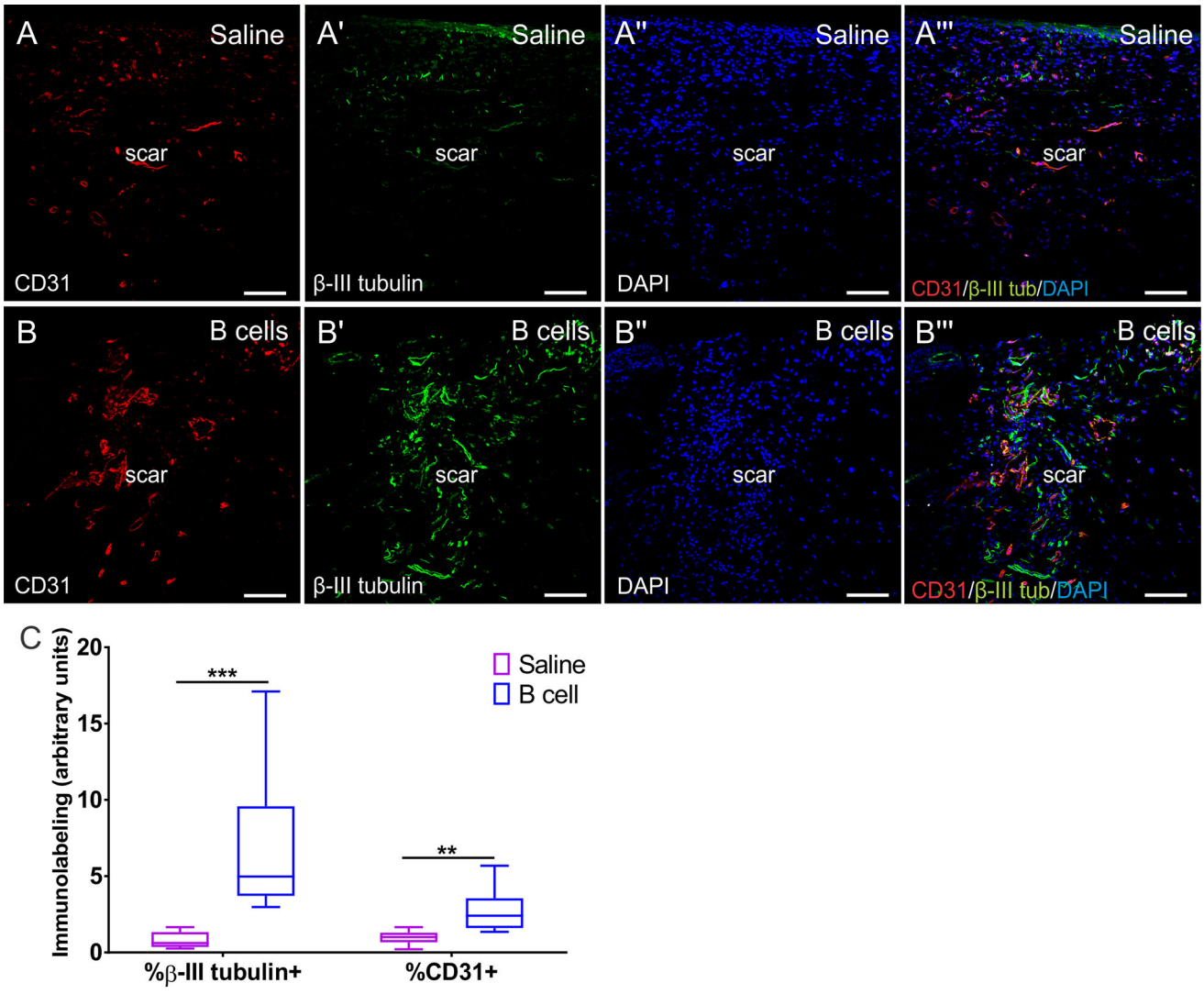

Figure 8. B cell application at the time of injury is associated with long-term increases in angiogenesis and nerve fiber growth in the scar tissue

A-A'" Confocal images of transverse sections through the scar tissue at 16 days post-injury in a saline treated (control) animal. At this time point, blood vessels ($CD31^+$) and nerve endings (β-III $tubulin^+$) have grown into the scar tissue. Cell nuclei are counterstained with DAPI. Scale bars, 100 μm. **B-B'"**. After B cell treatment at the time of injury, the scar at day 16 shows substantially more capillaries and blood vessels, as well as nerve endings. Scale bars, 100 μm. **C**. Quantitative assessment of the surface area covered by β-III $tubulin^+$ fibers or $CD31^+$ blood vessels normalized to $DAPI^+$ cell density, assessed in confocal fields of transverse sections through the scar tissue at day 16 post injury and treatment (n = 3 animals per condition; 3 fields from independent sections were analyzed for each animal). Analyses were performed using WT animals. Statistical significance was assessed using multiple t tests followed by Holm-Sidak correction for multiple comparisons. ** = $p < 0.01$; *** = $p < 0.001$.